nature chemical biology

ARTICLES

https://doi.org/10.1038/s41589-018-0031-6

$FINO_2$ initiates ferroptosis through GPX4 inactivation and iron oxidation

Michael M. Gaschler[1,9], Alexander A. Andia[2,9], Hengrui Liu[1], Joleen M. Csuka[3], Brisa Hurlocker[2], Christopher A. Vaiana[2], Daniel W. Heindel[2], Dylan S. Zuckerman[2], Pieter H. Bos[3], Eduard Reznik[3], Ling F. Ye[3], Yulia Y. Tyurina[4], Annie J. Lin[3], Mikhail S. Shchepinov[5], Amy Y. Chan[2], Eveliz Peguero-Pereira[2], Maksim A. Fomich[7], Jacob. D. Daniels[8], Andrei V. Bekish[6], Vadim V. Shmanai[7], Valerian E. Kagan[4], Lara K. Mahal[2], K. A. Woerpel[2]* and Brent R. Stockwell[1,3]*

Ferroptosis is a non-apoptotic form of regulated cell death caused by the failure of the glutathione-dependent lipid-peroxide-scavenging network. $FINO_2$ is an endoperoxide-containing 1,2-dioxolane that can initiate ferroptosis selectively in engineered cancer cells. We investigated the mechanism and structural features necessary for ferroptosis initiation by $FINO_2$. We found that $FINO_2$ requires both an endoperoxide moiety and a nearby hydroxyl head group to initiate ferroptosis. In contrast to previously described ferroptosis inducers, $FINO_2$ does not inhibit system x_c^- or directly target the reducing enzyme GPX4, as do erastin and RSL3, respectively, nor does it deplete GPX4 protein, as does FIN56. Instead, $FINO_2$ both indirectly inhibits GPX4 enzymatic function and directly oxidizes iron, ultimately causing widespread lipid peroxidation. These findings suggest that endoperoxides such as $FINO_2$ can initiate a multipronged mechanism of ferroptosis.

Regulated cell death includes several processes that lead to cell death through specific mechanisms that can be modulated with pharmacological and genetic tools. The recognition of cell death as a regulated process began with the discovery and characterization of apoptosis[1,2]. Ongoing work has since uncovered several other regulated cell death processes, including ferroptosis. Ferroptosis is an iron-dependent, oxidative form of regulated cell death that is distinct from apoptosis and is characterized by the failure of the glutathione (GSH)-dependent lipid peroxide defense network[3–5]. Consequently, cells undergoing ferroptotic cell death exhibit an increased accumulation of lipid peroxides and cannot be rescued by inhibitors of apoptosis or other cell death processes[6].

Organic peroxides, such as artemisinin (**1**) and artesunate (**2**), are used therapeutically as cytotoxic agents for the treatment of cancers[7–9]. Recently, development of analogs based on the plakinic acid natural products (**3**) identified the 1,2-dioxolane $FINO_2$ (**4**), which triggers ferroptosis (Fig. 1a)[10]. Further evaluation of ferroptosis induction by $FINO_2$ against multiple cancer lines revealed that $FINO_2$ selectively initiates ferroptosis in BJ-eLR cancer cells compared to the isogenic, noncancerous BJ-hTERT cell line[10]. Since evasion of apoptotic signaling is a hallmark of cancer[11], the ability of $FINO_2$ to initiate a non-apoptotic programmed cell death process selectively in tumorigenic cells makes it an attractive target for further study.

Here, we sought to define the mechanism by which $FINO_2$ induces ferroptosis and determine which structural features of $FINO_2$ are necessary for its function. These experiments demonstrate that, in contrast to other ferroptosis-inducing compounds such as erastin, $FINO_2$ does not deplete GSH through the inhibition of system x_c^-. $FINO_2$ instead bypasses GSH depletion to cause iron oxidation, as well as loss of activity of the lipid-peroxide-reducing enzyme GPX4 indirectly, by a mechanism that is distinct from that of other GPX4 inhibitors. Exploration of the structure–activity relationship around the $FINO_2$ scaffold revealed that both the endoperoxide moiety and the pendant hydroxyethyl group are necessary to induce oxidative events leading to ferroptotic cell death. We found that $FINO_2$ exerts dual effects involving iron oxidation and loss of GPX4 enzymatic activity to induce ferroptosis, and it therefore represents a distinct class of ferroptosis inducers.

Results

$FINO_2$ induces ferroptosis. We initially sought to evaluate the lethality of $FINO_2$ in a cell line in which ferroptosis had been previously examined. Ferroptosis-sensitive HT-1080 fibrosarcoma cells[3] were treated with a lethal concentration of $FINO_2$ (10 μM) (Supplementary Fig. 1a) alone or along with a panel of death-suppressing compounds at varied concentrations (Fig. 1b). The lethality of $FINO_2$ was suppressed by the ferroptosis inhibitor ferrostatin-1, which prevents the accumulation of lipid peroxides, likely through a radical-trapping mechanism[12,13]. Baicalein and Trolox, which have been reported to inhibit ferroptosis[6], both suppressed $FINO_2$ lethality (Fig. 1b). The apoptosis inhibitor zVAD-FMK was unable to suppress cell death. Necrostatin-1, an inhibitor of necroptosis, an alternative form of regulated cell death, was similarly unable to prevent $FINO_2$-induced death. We also evaluated the ability to suppress $FINO_2$ lethality of nitroxide antioxidants XJB-5-131 and JP4-039, which were previously found to suppress ferroptosis[14]. The mitochondria-targeted nitroxide XJB-5-131 was 39-fold more potent

[1]Department of Chemistry, Columbia University, New York, NY, USA. [2]Department of Chemistry, New York University, New York, NY, USA. [3]Department of Biological Sciences, Columbia University, New York, NY, USA. [4]Department of Environmental and Occupational Health, University of Pittsburgh, Pittsburgh, PA, USA. [5]Retrotope Inc, Los Altos, CA, USA. [6]Department of Chemistry, Belarusian State University, Minsk, Belarus. [7]Institute of Physical Organic Chemistry, National Academy of Sciences of Belarus, Minsk, Belarus. [8]Department of Pharmacology, Columbia University, New York, NY, USA. [9]These authors contributed equally: Michael M. Gaschler and Alexander A. Andia. *e-mail: kwoerpel@nyu.edu; bstockwell@columbia.edu

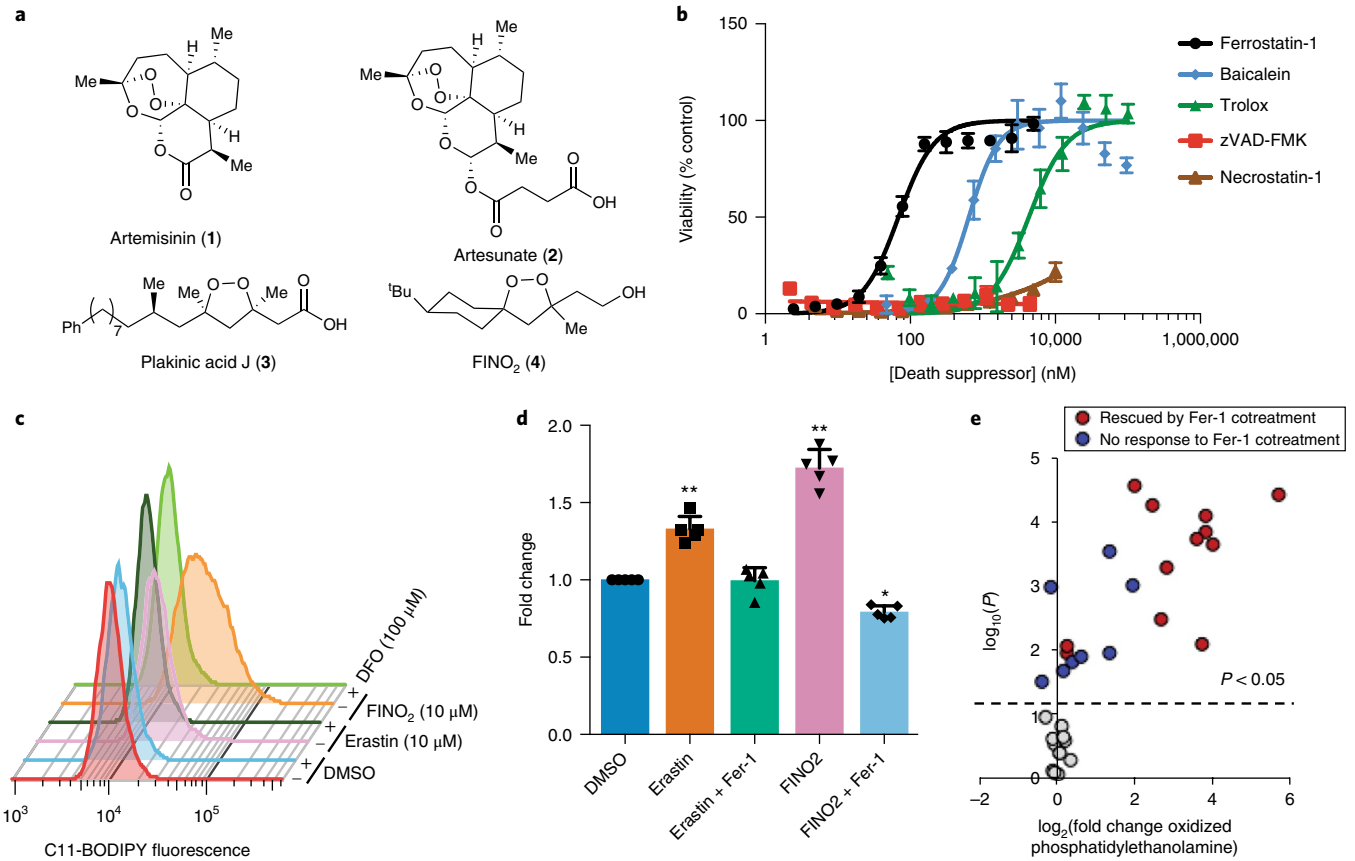

Fig. 1 | $FINO_2$ induces ferroptotic cell death. a, Organic peroxides and $FINO_2$. **b**, The dose-dependent effect of cell-death-suppressing compounds on ferroptosis triggered by $FINO_2$ (10 μM) in HT-1080 cells. Viability measured 24 h after compound treatment. Experiments were performed with triplicate cell cultures. Data are plotted as the mean ± s.d., $n = 3$. **c**, Ability of iron chelator DFO to prevent ferroptosis-dependent C11-BODIPY oxidation after 6 h incubation. Three independent experiments were performed with similar results. **d**, Ability of ferrostatin-1 (Fer-1) (2 μM) to prevent accumulation of TBARS when cotreated with erastin (5 μM) or $FINO_2$ (10 μM) for 6 h. Data are plotted as the mean ± s.d., $n = 5$. *P* values were determined using one-way ANOVA; $^*P = 0.003$, $^{**}P < 0.001$ versus DMSO control. **e**, Changes in oxidized PE abundance as detected by LC–MS after treatment with $FINO_2$ (10 μM) for 6 h. Individual lipid species are plotted with their $\log_2$(fold change in abundance) on the horizontal axis and the statistical significance of the change ($\log_{10}(P)$) on the vertical axis. *P* values were determined using two-sided *t*-tests. Lipid species with significant change upon $FINO_2$ treatment fall above the dashed line ($P < 0.05$). Experiments were performed in triplicate with biologically independent samples.

than the cytosolic JP4-039, highlighting the potential importance of mitochondrial lipid peroxidation in mediating $FINO_2$ lethality (Supplementary Fig. 1).

We next aimed to validate the finding that $FINO_2$ causes lipid peroxidation, a defining event in ferroptosis. HT-1080 cells were treated with either $FINO_2$ or the ferroptosis inducer erastin, and the increase in fluorescence intensity of the fluorescent lipid peroxidation probe C11-BODIPY was monitored by flow cytometry (Fig. 1c)[3]. Both erastin and $FINO_2$ showed an increase in fluorescence 6 h after treatment, with $FINO_2$ showing a much larger shift, suggesting that $FINO_2$ causes a more rapid onset or overall greater quantity of lipid peroxidation. This increase was suppressed by cotreatment with deferoxamine (DFO), an iron chelator, confirming the iron dependence of lipid peroxidation induced by both $FINO_2$ and erastin. We examined the oxidation of endogenous lipids by measuring the accumulation of thiobarbituric acid–reactive substances (TBARS) in cells treated with erastin or $FINO_2$ (Fig. 1d). This assay detects malondialdehyde, a common product from the degradation of multiple lipid species[15]. $FINO_2$-treated cells showed a greater increase in TBARS than did erastin. In both cases, cotreatment with ferrostatin-1 suppressed TBARS accumulation, indicating the presence of lipid peroxidation suppressible by a specific ferroptosis inhibitor.

To gain insight into the type of lipid oxidation caused by $FINO_2$, we used liquid chromatography–mass spectrometry (LC–MS) analysis to measure the oxidation of phosphatidylethanolamine (PE), a lipid critical to the propagation of ferroptosis (Fig. 1e and Supplementary Fig. 2)[16]. $FINO_2$ treatment caused a large increase in a diverse set of oxidized PE species. Not all PEs that were oxidized in response to $FINO_2$ had their oxidation suppressed by cotreatment with ferrostatin-1, suggesting that only a specific set of oxidized PE species contribute to ferroptosis.

$FINO_2$ does not alter glutathione homeostasis. Having validated the finding that $FINO_2$ causes ferroptosis in HT-1080 cells, we sought to define the mechanism by which $FINO_2$ induces ferroptosis in these cells. Originally, ferroptosis-inducing compounds were divided into two classes. Class 1 ferroptosis inducers decrease intracellular GSH, a necessary cofactor for the lipid-peroxide-reducing enzyme GPX4. Class 2 ferroptosis inducers inhibit GPX4 directly through active site inhibition. More recently, the small molecule FIN56 was reported to deplete GPX4 protein and also to deplete coenzyme Q10, an endogenous inhibitor of lipid peroxidation, through modulation of the mevalonate pathway[17].

A major source of cysteine for GSH synthesis is the cystine/glutamate antiporter, system x_c^- (Supplementary Fig. 3). Inhibition of

system x_c^- by erastin, sulfasalazine, sorafenib or glutamate depletes intracellular GSH and induces ferroptosis[18]. To test whether $FINO_2$ acts via system x_c^- inhibition and GSH depletion, we examined the ability of $FINO_2$ to inhibit system x_c^- function using a fluorescent enzymatic assay that quantifies the amount of glutamate released by cells into glutamate-free medium (Fig. 2a)[18]. Both erastin and sulfasalazine were able to inhibit glutamate release compared to vehicle-treated cells. $FINO_2$ showed minimal inhibition of glutamate release, suggesting that inhibition of system x_c^- is not a primary mechanism of $FINO_2$ lethality. We also quantified glutathione in cells undergoing ferroptosis using a reactive fluorescent reporter of free thiols in cell lysates (Fig. 2b). To eliminate nonspecific reactivity with accessible cysteine residues on proteins, we precipitated the protein fraction of lysates, leaving GSH as the major thiol in solution[19]. Cells treated with erastin exhibited a threefold decrease in GSH content compared to cells treated with vehicle or the GPX4 inhibitor (1*S*,3*R*)-RSL3, hereafter referred to as RSL3. $FINO_2$-treated cells showed no decrease in thiol content, indicating that $FINO_2$ does not deplete GSH. These results suggest that $FINO_2$ is not a system x_c^- inhibitor and does not deplete GSH through other mechanisms.

The oxidative stress caused by erastin upregulates components of the endoplasmic reticulum (ER) stress response pathway. The GSH-specific γ-glutamylcyclotransferase enzyme encoded by the *CHAC1* gene has been observed to be a pharmacodynamic marker of exposure to erastin[18]. To test whether $FINO_2$ induces transcriptional changes similar to those of other ferroptosis inducers, we performed reverse transcription and quantitative PCR to quantify the amount of *CHAC1* mRNA in cells treated with erastin or $FINO_2$ (Fig. 2c). Cells treated with $FINO_2$ showed a sevenfold increase in *CHAC1* mRNA compared to vehicle. This upregulation was nearly threefold less than the upregulation in cells treated with erastin. This more modest upregulation indicates that $FINO_2$ induces different transcriptional responses than an equivalent concentration of erastin.

$FINO_2$ indirectly inhibits GPX4 activity in cells. Because $FINO_2$ does not display the characteristic functional or genetic hallmarks of a class 1 ferroptosis inducer, we next evaluated the ability of $FINO_2$ to act as a class 2 ferroptosis inducer by inhibiting GPX4 enzymatic activity. GPX4 is a selenocysteine-containing enzyme responsible for reducing lipid hydroperoxides to lipid alcohols, making it a master regulator of ferroptotic signaling (Supplementary Fig. 3). To understand the impact of $FINO_2$ on GPX4 activity, we used an LC–MS–based assay to monitor the ability of GPX4-containing lysates collected from cells treated with vehicle or ferroptosis inducers to reduce the GPX4-specific substrate phosphatidylcholine hydroperoxide (PCOOH) (Supplementary Fig. 4)[4,17]. Whereas erastin-treated cells did not show reduced GPX4 activity in this assay, treatment of cells with $FINO_2$, FIN56 or RSL3 decreased the activity of GPX4 in the resulting lysates to a similar extent. We next monitored the kinetics of GPX4 inhibition by RSL3 and $FINO_2$ by varying the amount of time cells were incubated with either compound. We observed that RSL3 caused a more rapid inhibition of GPX4 activity than did $FINO_2$ (Supplementary Fig. 5), suggesting that $FINO_2$ might have a distinct mechanism of action from RSL3.

The observation that $FINO_2$ caused decreased GPX4 activity suggested that, like RSL3, $FINO_2$ might be a direct inhibitor of GPX4[4,6] or that $FINO_2$ could deplete GPX4 protein, similarly to the ferroptosis inducer FIN56[17]. To test whether $FINO_2$ is a direct inhibitor of GPX4, we again used the LC–MS–based PCOOH reduction assay to monitor the reduction of PCOOH in GPX4-containing cell lysates treated with ferroptosis inducers after cell lysis (Fig. 3a). Because ferroptosis inducers are added after cell lysis, only molecules capable of directly inhibiting active GPX4 can prevent PCOOH reduction. As expected, the direct GPX4 inhibitor RSL3 was able to prevent PCOOH reduction in this assay (Fig. 3a). $FINO_2$ was unable to prevent PCOOH reduction, even at elevated concentrations, suggesting that $FINO_2$ is not a direct inhibitor of GPX4. To support our hypothesis that $FINO_2$ does not directly interact with GPX4, we performed ^1H-^{15}N heteronuclear single quantum coherence (HSQC) NMR spectroscopy on $GPX4^{U46C}$ in the presence and absence of $FINO_2$. Unlike RSL3, $FINO_2$ did not cause a change in the HSQC spectrum of GPX4, indicating that $FINO_2$ is neither an allosteric nor active site ligand of GPX4 (Fig. 3b and Supplementary Fig. 6).

Gene *PTGS2*, which encodes prostaglandin synthase, is upregulated following RSL3 treatment[4]. We determined whether cells experienced a similar upregulation following treatment with $FINO_2$. $FINO_2$ and erastin showed less upregulation of *PTGS2*, than RSL3, indicating that FINO does not cause the same transcriptional changes as the class 2 ferroptosis inducer RSL3 (Fig. 3c).

To evaluate whether $FINO_2$ acts as an irreversible covalent inhibitor of GPX4, HT-1080 cells were treated with a lethal dose of each ferroptosis inducer and either vehicle, ferrostatin-1 or β-mercaptoethanol (β-ME) (Fig. 3d). In the extracellular medium, β-ME reacts with cystine to form a disulfide bond with cysteine. Neutral amino acid transporters import this mixed disulfide, bypassing system x_c^- and increasing intracellular cysteine availability[20]. When cells are cotreated with RSL3 and β-ME, the increase in cysteine availability for GSH synthesis is unable to rescue cells because GPX4 is irreversibly and covalently inhibited. Conversely, the lethality of

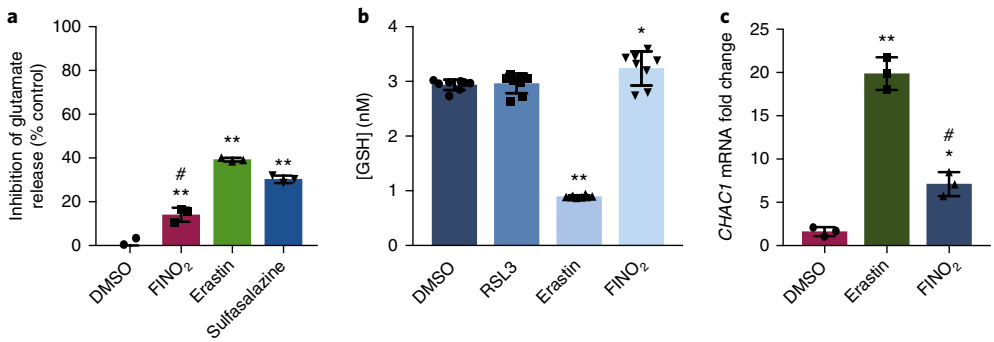

Fig. 2 | $FINO_2$ does not alter glutathione homeostasis. a, Effect of $FINO_2$ (10 μM) and system x_c^- inhibitors erastin (10 μM) and sulfasalazine (1 mM) on glutamate release after 1 h incubation. Data are plotted as the mean ± s.d., $n = 3$ biologically independent samples. $^{**}P < 0.001$ and $^{\#}P < 0.001$ versus DMSO control and erastin, respectively. **b**, Intracellular GSH levels in HT-1080 cells treated with ferroptosis inducers RSL3 (0.5 μM) for 90 min, or erastin (5 μM) or $FINO_2$ (10 μM) for 6 h; data are plotted as the mean ± s.d., $n = 8$ biologically independent samples. $^{*}P = 0.016$, $^{**}P < 0.001$ versus DMSO control. **c**, *CHAC1* mRNA levels following erastin (10 μM) or $FINO_2$ (10 μM) treatment for 6 h. Data are plotted as the mean ± s.d., $n = 3$ biologically independent samples. $^{*}P = 0.007$, $^{**}P < 0.001$ versus DMSO control; $^{\#}P < 0.001$ versus erastin. All *P* values were determined using one-way ANOVA.

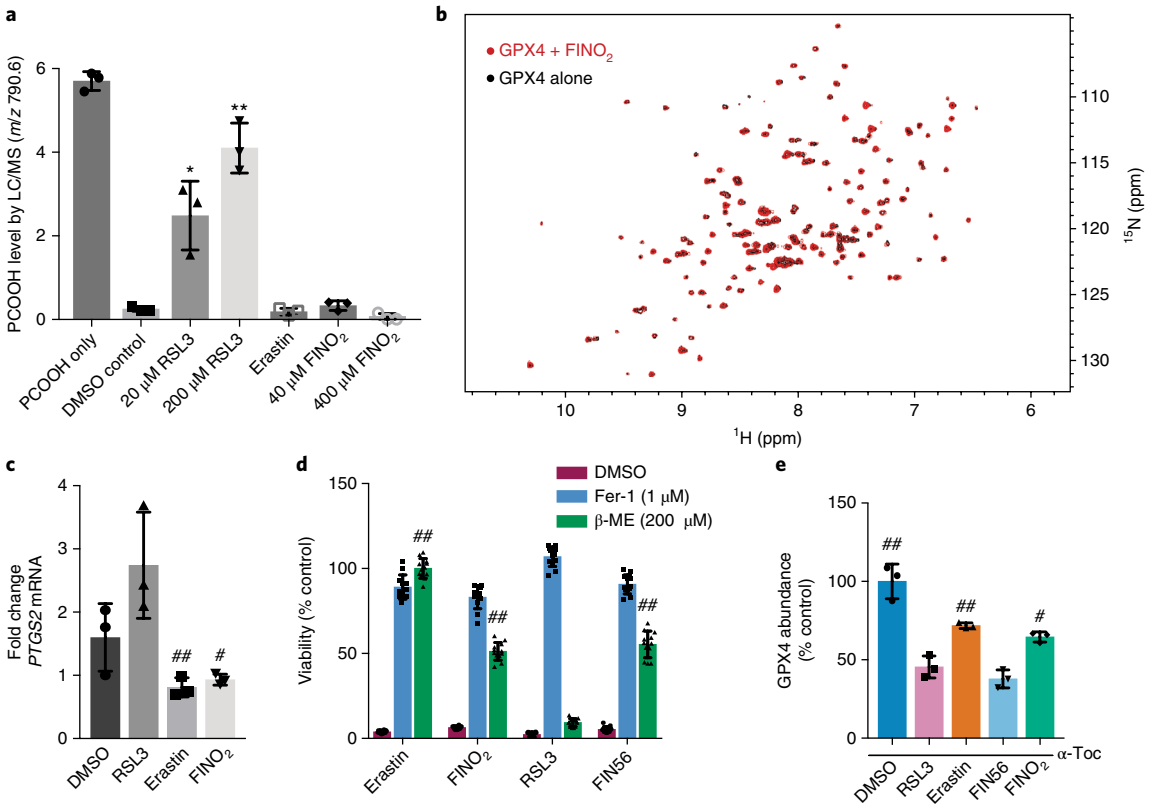

Fig. 3 | $FINO_2$ indirectly inhibits GPX4 activity. a, Effect of ferroptosis inducers on GPX4 activity within the GPX4-containing cell lysates. Cell lysates were treated with PCOOH and GSH and the abundance of PCOOH was measured by LC–MS. Data are plotted as the mean ± s.d., $n = 3$ biologically independent samples. $^{*}P = 0.009$, $^{**}P < 0.001$ versus DMSO control. **b**, HSQC spectrum of GPX4 protein (black; 50 μM) overlaid with the spectrum of GPX4 incubated with $FINO_2$ for 6 h (red; 50 μM GPX4 and 500 μM, $FINO_2$). **c**, *PTGS2* mRNA levels following treatment with RSL3 (0.5 μM), erastin (10 μM) and $FINO_2$ (10 μM) for 6 h. Data are plotted as the mean ± s.d., $n = 3$ biologically independent samples. $^{\#}P = 0.021$, $^{\#\#}P = 0.017$ versus RSL3. **d**, Ability of β-ME to prevent ferroptosis initiated by different inducers. Viability measured 24 h after treatment. Data are plotted as the mean ± s.d., $n = 12$ biologically independent samples. $^{\#\#}P < 0.001$ versus RSL3. **e**, GPX4 protein abundance in HT-1080 cells cotreated with RLS3 (1 μM), erastin (10 μM), FIN56 (5 μM) or $FINO_2$ (10 μM) and 100 μM α-tocopherol for 10 h. Data are plotted as the mean ± s.d., $n = 3$ biologically independent samples. $^{\#}P = 0.002$, $^{\#\#}P < 0.001$ versus FIN56. Representative blot image is shown in Supplementary Fig. 7. All *P* values were determined using unpaired two-tailed Student's *t*-test.

erastin is fully suppressed by β-ME, as cysteine availability is no longer dependent on system x_c^- function. β-ME also rescued ferroptosis induced by FIN56, which depletes GPX4 protein abundance (Fig. 3d)[17]. β-ME may prevent FIN56 lethality by increasing the cysteine available for GSH synthesis, thereby improving the activity of the remaining GPX4[21]. Ferroptosis induced by $FINO_2$ was partially rescued by β-ME, further indicating that $FINO_2$ is not an irreversible covalent inhibitor of GPX4. Since $FINO_2$ does not decrease intracellular glutathione (Fig. 2b), we reasoned that β-ME supplementation might rescue $FINO_2$-treated cells by enhancing GPX4 activity, similarly to the situation with FIN56.

To test whether $FINO_2$ causes GPX4 protein depletion similarly to FIN56, we quantified the abundance of GPX4 protein in cells undergoing ferroptosis by western blotting (Fig. 3e and Supplementary Fig. 7). As expected, both RSL3 and FIN56 caused a large decrease in the abundance of GPX4 at the protein level[17]. Erastin and $FINO_2$ caused only a minor decrease in GPX4 protein abundance, suggesting that $FINO_2$ is unlike FIN56.

The endoperoxide moiety is required for $FINO_2$ lethality. Since $FINO_2$ does not display behavior characteristic of a class 1 or class 2 ferroptosis inducer, we sought to gain insight into its mechanism by determining which functional groups in $FINO_2$ are required for inducing ferroptosis. Earlier reports indicated that the ether linkage in artemisinin dimers may be more critical for cytotoxic activity than the endoperoxide component[22,23]. Therefore, we prepared a series of nonperoxide derivatives of $FINO_2$.

The first derivatives synthesized possessed a spirocyclic oxetane unit. These derivatives can be viewed as analogs in which an oxygen atom was removed from the peroxide functional group. Earlier studies indicate that spirocyclic oxetanes, which are emerging as effective drug candidates, are cytotoxic toward cancer cells[24,25]. The spirocyclic oxetanes were synthesized from cyclohexanones **5**–**7** in three steps. Addition of allylmagnesium chloride afforded alkenes **8**–**10**[26,27]. Treatment of these alkenes with *meta*-chloroperoxybenzoic acid (-*m*CPBA) yielded epoxides **11**–**13**. These epoxides were then heated under basic conditions to afford oxetanes **14**–**16**[28]. During attempts to synthesize the *O*-axial diastereomers, however, rapid elimination of water occurred under the strongly basic conditions required for cyclization[29].

Similar methodology was used to prepared tetrahydrofuran derivatives of $FINO_2$. These furans were selected because they maintain the same-sized rings as found in $FINO_2$ while removing the peroxide functional group. Terpenoid-derived spirocyclic furans are reported to induce apoptosis in a range of cancers, with half-maximal inhibitory concentration values in the low micromolar range[30]. Other fused-ring furans have shown biological activity for a range of diseases[31]. The spirocyclic furan derivatives were prepared from cyclohexanone **5** in two steps. Homoallylation of ketone **5** afforded alkenes **17a** and **17b**. Upon exposure to the epoxidation

conditions, tetrahydrofurans **18a** and **18b** were formed. This intramolecular cyclization is likely to occur by cyclization of the hydroxyl group onto a protonated epoxide intermediate[32]. Avoiding the basic cyclization step allowed us to prepare a $FINO_2$ derivative with an axial oxygen atom (**18a**).

Another derivative of $FINO_2$ was synthesized by ring expansion. Hydrogenation of the oxygen–oxygen bond in $FINO_2$ yielded triol **19**. Subsequent protection of this triol with benzyl bromide occurred only at the primary hydroxyl group, forming 1,3-diol **20**. Protection of this 1,3-diol with dibromomethane afforded 1,3-dioxane **21**. Deprotection of the benzyl group yielded the desired 1,3-dioxane analog **22**. We considered triol **19** to also be an analog of $FINO_2$ that warranted cell studies. Considering the reducing environment of the cell[33], $FINO_2$ could act as a prodrug, forming triol **19**. Thus, the activity of $FINO_2$ could be due to the reduced product, as observed for some other peroxide-based drugs[34,35].

We measured the activities of $FINO_2$ and its analogs in several cell lines. These cells included the renal cancer cell line CAKI-1 and two immortalized fibroblast cell lines, BJ-hTERT and its tumorigenic counterpart BJ-eLR. Activities were measured using the CellTiter-Glo assay (Fig. 4a). In all cases, the nonperoxide compounds displayed essentially no activity. $FINO_2$, however, was able to kill oncogenic BJ-eLR and CAKI-1 cells selectively compared to BJ-hTERT cells. This result suggested that the peroxide moiety was essential for the induction of ferroptosis.

Earlier studies have also reported biological activity of 1,2-dioxolane-containing natural products, such as the plakinic acids and plakortides[36,37]. To determine the general ability of 1,2-dioxolanes to initiate ferroptosis, we synthesized a series of peroxide-containing $FINO_2$ analogs. These synthetic analogs had modifications of both the hydrophobic and hydrophilic moieties while retaining the 1,2-dioxolane core. The 1,2-dioxolanes were synthesized from ketones **5**–**7** and **34**. Treatment with LiN^iPr_2 yielded silyl enol ethers **23**–**25** and **35**[38]. Regioselective cobalt-catalyzed peroxidation of these products furnished mixed peroxyketals **26**–**28** and **36**[38]. Treatment of these compounds with 5 mol% of $SnCl_4$ and alkene **29**, **30**, **38** or **40** followed by immediate deprotection yielded $FINO_2$ (**4**) and derivatives **31**–**33**, **37**, **39** and **41**[38].

These 1,2-dioxolanes were tested in the renal cancer cell line (CAKI-1) along with both 10,12-peroxycalamenene (**42**)[37] and artemisinin (**1**) (Fig. 4b). We selected these natural products because 10,12-peroxycalamenene has been shown to induce apoptosis in human breast carcinoma cells[39], and several studies have reported on artemisinin's activity against cancer[7–9,40–42].

The structure–activity relationship studies suggest that $FINO_2$ belongs to a class of ferroptosis-inducing compounds that are somewhat tolerant of modifications while retaining biological activity, unlike RSL3. Moving the *tert*-butyl group of $FINO_2$ from C-4 to C-3 (**31**) resulted in a small decrease in potency. Removing the polar functionality (**32**) revealed that, although a peroxide moiety is necessary for initiating ferroptosis, it is not sufficient. Increasing the distance between the peroxide bond and hydroxyl group (**41**) also resulted in a decrease in activity. These data demonstrate that the hydroxyl portion of $FINO_2$ must be present and have a specific spatial relationship to the peroxide, suggesting a specificity of mechanism for $FINO_2$. Observations of cytotoxic activity of naturally occurring peroxides noted a similar requirement[37].

The *tert*-butyl group, which can be metabolically unstable[43], is not required. When that group was replaced with an aromatic ring, 1,2-dioxolane **33** was similarly potent. Retaining the spirobicyclic core structure of $FINO_2$ was also not necessary. Monocyclic peroxide **37**, an analog that resembles plakinic acid J (**3**) (Fig. 1a), displayed activity similar to $FINO_2$. The activity of **37** suggests that the cytotoxicity of **3** may be due to ferroptosis, not apoptosis[36,37]. As observed for peroxide natural products[37], hydrophobic analog **39** was also inactive.

$FINO_2$ is a stable oxidant that oxidizes ferrous iron. Since the peroxide moiety in $FINO_2$ is necessary for inducing ferroptosis, we hypothesized that $FINO_2$ might be a selective pro-oxidant molecule that initiates ferroptosis through specific oxidation of ferroptosis-relevant substrates. Consistent with this hypothesis of relative inertness to most substrates, $FINO_2$ was previously determined to be stable to 150 °C by thermogravimetric analysis[10]. Similar 1,2-dioxolanes have also shown stability to $LiBH_4$ and $LiEt_3BH$, strong hydride reducing agents, at room temperature[44].

Subjection to these high temperatures and strong reducing conditions, however, are not necessarily biologically relevant. We therefore subjected $FINO_2$ to a variety of biologically relevant redox conditions in vitro (Supplementary Fig. 8) and monitored for reaction by ^{1}H-NMR spectroscopy. Heating $FINO_2$ at 37 °C with a thiol, a class of compounds that are typically found at 0.5–10 mM in human cells[19], yielded no decomposition. $FINO_2$ was found to be stable to GSH, in agreement with the observation that $FINO_2$ did not deplete GSH (see above). Arachidonic acid, a ubiquitous polyunsaturated fatty acid in cell membranes, showed no degradation following treatment with $FINO_2$. Selenium-containing compounds such as selenocysteine and ebselen, the latter of which is a model

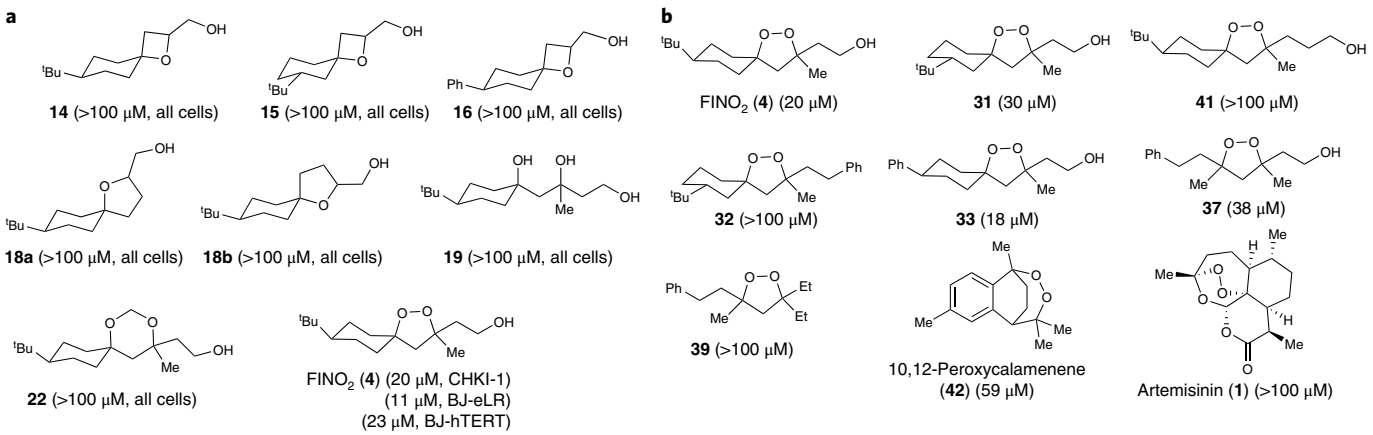

Fig. 4 | Potency of analogs. a,**b**, Potency of nonperoxide analogs (**a**) and peroxide analogs (**b**) of $FINO_2$. BJ-eLR, BJ-hTERT or CAKI-1 cells were treated with either vehicle (DMSO), $FINO_2$ or a $FINO_2$ analog at 5, 10, 25, 50 or 100 μM for 48 h. Cell viability was then measured and normalized to the DMSO vehicle to extract half-maximal effective concentration (EC_{50}) values. EC_{50} values are shown in parentheses. Compounds **15**, **31**, **32** and **37** were tested as mixtures of diastereomers.

for GPX4[45], also did not reduce the peroxide bond. The inability of ebselen to reduce $FINO_2$ is consistent with the observation that GPX4 cannot reduce endoperoxides[46]. Ebselen was only able to reduce $FINO_2$ at 90 °C, which suggests that $FINO_2$ does not readily degrade to its reduced form **19** or to reactive oxygen species to confer biological activity. These results, along with the lack of reactivity toward most reducing agents, suggest that the intact endoperoxide form is responsible for activity.

$FINO_2$ was also stable at varying pH. No reaction was observed with amines or strong bases, even under conditions beyond the basicity found in peroxisomes[47]. $FINO_2$ was also found to be stable under acidic conditions that mimic conditions found in lysosomes[48]. To examine the stability of $FINO_2$ in biological systems, we measured the stability of $FINO_2$ in human and mouse plasma and liver microsomes. We found that $FINO_2$ had high stability in plasma and human microsomes (Supplementary Fig. 9).

Analogously to Fenton chemistry, 1,2-dioxolanes and ferrous iron can generate oxygen-centered radicals that initiate oxidative damage in biological systems[44]. We hypothesized that $FINO_2$ might initiate Fenton-type chemistry selectively over other organic peroxides[3,12]. Using an in vitro colorimetric assay, we monitored the oxidation state of iron treated with oxidizing compounds (Fig. 5a). Out of all tested organic peroxides, only $FINO_2$ and *tert*-butyl hydroperoxide (^{t}BuOOH) were able to oxidize ferrous iron in vitro (Fig. 5a). Cell death initiated by ^{t}BuOOH cannot be suppressed by ferrostatin-1 or β-ME (Supplementary Fig. 10), indicating that the lethality of ^{t}BuOOH cannot be attributed to ferroptosis.

The iron oxidation by $FINO_2$ is accompanied by a degradation of the endoperoxide. Incubation of $FINO_2$ at 37 °C for 12 h reveals reduction of the peroxide bond by $FeSO_4$, as seen in similar systems (Fig. 5b)[49]. This reduction is consistent with studies on 1,2,4-trioxolanes and plakortin derivatives that suggest rapid reduction of the peroxide functionality[34,35,49,50]. Consistent with previous studies, artesunate (**2**) also decomposed after exposure to iron (Supplementary Fig. 11)[7]. Inactive analogs **32** and **41** were only partially decomposed after iron exposure (Supplementary Fig. 11). These results suggest that the complete breakdown of the peroxide moiety by iron is required to induce ferroptosis.

The selectivity of iron oxidation by $FINO_2$ compared to analogs **32** and **41** suggested that iron oxidation might be important to ferroptosis initiation by $FINO_2$. The iron chelator DFO is able to suppress the lethality of $FINO_2$ tenfold more potently than that of erastin or RSL3 (Fig. 5c). Similarly, supplementation of cell medium with ferrous or ferric salts sensitized cells to $FINO_2$-initiated ferroptosis, but not to RSL3-initiated ferroptosis (Supplementary Fig. 12). Despite the apparent importance of iron to $FINO_2$ lethality, $FINO_2$ treated cells did not show changes in the abundance of the iron regulatory proteins IRP2, FTL1 or TFR (Supplementary Fig. 13), suggesting that $FINO_2$ may engage labile cellular iron preferentially over iron-containing proteins.

$FINO_2$ oxidizes the lipidome independent of ALOX activity. Previously, the family of arachidonic acid lipoxygenases (ALOX) was shown to be critical in generating lipid peroxides during ferroptosis, particularly in response to erastin or RSL3[6]. siRNA knockdown of either the *ALOX15B* or *ALOXE3* genes suppressed the lethality of erastin. Similarly, a GFP-ALOX5 fusion protein expressed in ferroptosis-sensitive cells was activated and translocated to the nuclear membrane following erastin treatment. Because $FINO_2$ is able to oxidize ferrous iron directly, we sought to evaluate whether ferroptosis initiated by $FINO_2$ required enzymatic lipid peroxidation, similarly to that initiated by erastin and RSL3. We assembled a collection of arachidonic acid derivatives deuterated at the bis-allylic positions. Deuteration at the bis-allylic position creates a strong kinetic isotope effect in lipoxygenase enzymes, making deuterated arachidonic acids effective and highly specific inhibitors of lipoxygenases (Fig. 6a).

We incubated HT-1080 cells with vehicle only (0.1% ethanol), arachidonic acid or a deuterated arachidonic acid overnight to allow incorporation of the fatty acid into cellular membranes. Cells were then treated with erastin, RSL3 or $FINO_2$ (Fig. 6b). Deuteration at the 7 position was strongly protective against cell death initiated by erastin and RSL3, confirming the importance of ALOX5 in initiating ferroptosis for these molecules. Ferroptosis induced by $FINO_2$ was only weakly rescued by deuteration at the 7 position, suggesting that $FINO_2$ either activates an ALOX isoform with different regioselectivity or preferentially oxidizes fatty acid groups other than arachidonic acid. To evaluate whether $FINO_2$ activates a different lipoxygenase isoform than erastin or $FINO_2$, we tested all combinations of deuterated arachidonic acid analogs against all ferroptosis inducers. Additional deuteration increased the amount of death suppression for erastin and RSL3, and the fully deuterated D_6-arachidonic acid completely suppressed the lethality of both of these ferroptosis inducers. No significant suppression of ferroptosis initiated by $FINO_2$ was observed for any deuterated arachidonic acid tested (Fig. 6b), suggesting that $FINO_2$ does not require ALOX-mediated peroxidation for ferroptosis induction.

To compare the global lipidomic changes following treatment with $FINO_2$ or erastin, we used LC–MS to identify oxidized esterified phospholipids extracted from HT-1080 cells treated with vehicle (DMSO), $FINO_2$ or erastin with and without ferrostatin-1. Because of its importance to ferroptosis, we first compared the

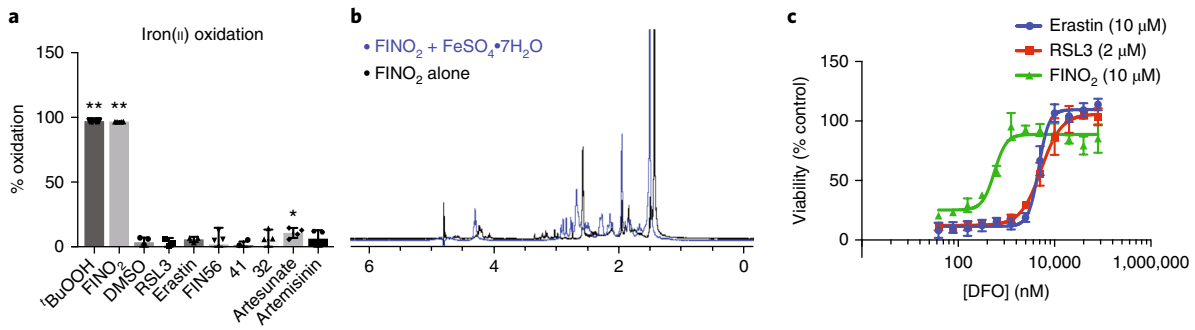

Fig. 5 | $FINO_2$ directly oxidizes ferrous ion. a, Oxidation of ferrous iron (500 μM) in the presence of different oxidizing agents (500 μM). Data are plotted as the mean ± s.d., $n = 4$ biologically independent samples. *P* values were determined using unpaired two-tailed Student's *t*-test. $^*P = 0.035$, $^{**}P < 0.001$ versus DMSO control. **b**, ^{1}H-NMR showing degradation of $FINO_2$ following incubation with $FeSO_4{\cdot}7H_2O$ in CD_3CN/D_2O (1:1) for 12 h. **c**, Ability of iron chelator DFO to inhibit ferroptosis initiated by different inducers. Experiments were performed in triplicate with three biologically independent samples. Data are plotted as the mean ± s.d.

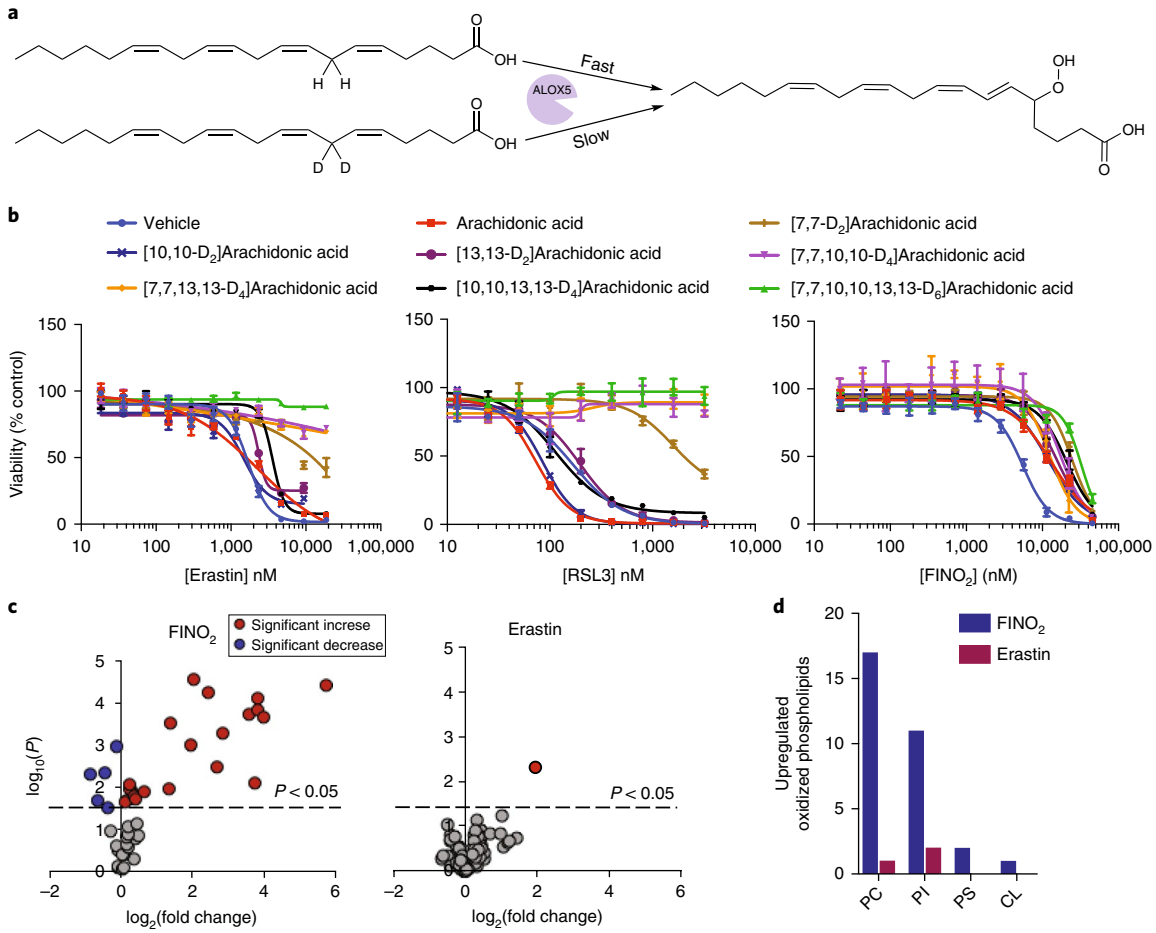

Fig. 6 | Ferroptosis initiated by $FINO_2$ oxidizes a large subset of the lipidome independent of lipoxygenase activity. a, Schematic of lipoxygenase inhibition by deuterated arachidonic acid. **b**, Effect of deuterated arachidonic acid incubation (80 μM for 24 h) on HT-1080 sensitivity to ferroptosis inducers. Experiments were performed in triplicate with biologically independent samples. Data are plotted as the mean ± s.d. **c**, Volcano plots showing the change in abundance of oxidized PE species in HT-1080 cells following incubation with $FINO_2$ (10 μM) or erastin (5 μM) for 6 h. Red circles indicate significant increase in abundance; blue circles indicate a significant depletion following treatment. Experiments were performed in triplicate with biologically independent samples. *P* values were determined using two-sided *t*-test. Lipid species with significant change upon $FINO_2$ treatment fall above the dotted line ($P < 0.05$). **d**, Number of oxidized phosphatidylcholine (PC), phosphatidylinositol (PI), phosphatidylserine (PS) and cardiolipin (CL) species upregulated in HT-1080 cells following treatment with $FINO_2$ (10 μM) or erastin (5 μM) for 6 h.

changes in oxidized PE following treatment with either ferroptosis inducer at equivalent time points (Fig. 6c). Whereas erastin caused an increase in 1 PE species after treatment, $FINO_2$ caused an increase in 21 PE species (Supplementary Fig. 2). This pattern was consistent for other phospholipids, including phosphatidylcholine, phosphatidylinositol, phosphatidylserine and cardiolipin (Fig. 6d). The increases in oxidized phosphatidylserine and cardiolipin were unresponsive to ferrostatin treatment, suggesting they do not contribute to ferroptosis (Supplementary Fig. 2b). MS analysis allowed us to identify the acyl tail portions of the oxidized phospholipids. As expected, all acyl tails contained some degree of polyunsaturation. Many of the oxidized phospholipids contained linoleic (18:2), arachidonic (20:4) and other polyunsaturated moieties. Cumulatively, these data show that $FINO_2$ causes the oxidation of a much more diverse set of phospholipids than does erastin, and does not have strong substrate selectivity within the set of polyunsaturated lipids.

Discussion

A common feature of all ferroptosis inducers is the ability to overcome the endogenous GSH-dependent lipid peroxidation defense network. In this study, we investigated the mechanism by which the 1,2-dioxolane $FINO_2$ is able to induce ferroptosis in cells. $FINO_2$ did not elicit the same transcriptional, translational and phenotypic responses expected from previously described ferroptosis inducers. We hypothesize that $FINO_2$ is able to initiate ferroptosis through a combination of its abilities to directly oxidize labile iron and inactivate GPX4.

In support of this hypothesis, we found that the highly oxidizing peroxide group and a nearby polar head group were both required for lethality and for oxidation of ferroptosis-relevant substrates. Neither nonperoxide derivatives nor nonpolar derivatives of $FINO_2$ were lethal to cells. Elongation of the polar head group led to a loss in activity as well as an inability to oxidize iron, suggesting that the spatial relationship between the peroxide and hydroxyl moieties in $FINO_2$ is required to engage labile iron or may facilitate the reduction of the oxygen–oxygen bond. Ferroptosis initiation by $FINO_2$ is highly sensitive to iron availability and involves oxidation of a broad set of polyunsaturated lipids. Unlike other peroxide-containing compounds, $FINO_2$ is able to initiate ferroptosis preferentially over other forms of cell death. Multiple factors could account for this remarkable selectivity, including inactivation of GPX4 or the lipophilicity of $FINO_2$. The predicted octanol/water partition

coefficient (Slog*P*) for $FINO_2$ is 3.54, whereas the value for artemisinin is 2.39, making $FINO_2$ more than an order of magnitude more lipophilic than artemisinin. Because of its high lipophilicity, $FINO_2$ may accumulate in the appropriate lipid bilayers of cell membranes, allowing it to oxidize polyunsaturated fatty acids directly in the locations that trigger ferroptosis.

In summary, this study provides insight into the mechanism of ferroptosis by $FINO_2$ and offers new perspectives on how ferroptosis can be initiated. Structural exploration of $FINO_2$ and its analogs revealed that this new class of ferroptosis inducer can be modified and retain biological activity, but requires the endoperoxide and hydrophilic head to be present. In addition, whereas previous ferroptosis initiators inhibited components of the endogenous lipid-peroxide-scavenging network in cells, $FINO_2$ induces ferroptosis through a combination of direct oxidation of ferroptosis-relevant substrates and indirect GPX4 inactivation. The mechanism of GPX4 inactivation by $FINO_2$ remains unclear, since $FINO_2$ does not decrease levels of GPX4 protein and is not a GPX4 ligand. Nonetheless, we hypothesize that this specific combination of pro-oxidant functionality and GPX4 inactivation is required to navigate cells to ferroptosis in response to this class of compounds.

Methods

Methods, including statements of data availability and any associated accession codes and references, are available at https://doi.org/10.1038/s41589-018-0031-6.

Received: 21 June 2017; Accepted: 14 February 2018;
Published online: 02 April 2018

References

1. Elmore, S. Apoptosis: a review of programmed cell death. *Toxicol. Pathol.* **35**, 495–516 (2007).
2. Lockshin, R. A. & Zakeri, Z. Programmed cell death and apoptosis: origins of the theory. *Nat. Rev. Mol. Cell. Biol.* **2**, 545–550 (2001).
3. Dixon, S. J. et al. Ferroptosis: an iron-dependent form of nonapoptotic cell death. *Cell* **149**, 1060–1072 (2012).
4. Yang, W. S. et al. Regulation of ferroptotic cancer cell death by GPX4. *Cell* **156**, 317–331 (2014).
5. Cao, J. Y. & Dixon, S. J. Mechanisms of ferroptosis. *Cell. Mol. Life. Sci.* **73**, 2195–2209 (2016).
6. Yang, W. S. et al. Peroxidation of polyunsaturated fatty acids by lipoxygenases drives ferroptosis. *Proc. Natl. Acad. Sci. USA* **113**, E4966–E4975 (2016).
7. Crespo-Ortiz, M. P. & Wei, M. Q. Antitumor activity of artemisinin and its derivatives: from a well-known antimalarial agent to a potential anticancer drug. *J. Biomed. Biotechnol.* **2012**, 247597 (2012).
8. Li, Z., Li, Q., Wu, J., Wang, M. & Yu, J. Artemisinin and its derivatives as a repurposing anticancer agent: what else do we need to do? *Molecules* **21**, 1331 (2016).
9. Krishna, S. et al. A randomised, double blind, placebo-controlled pilot study of oral artesunate therapy for colorectal cancer. *EBioMedicine* **2**, 82–90 (2014).
10. Abrams, R. P., Carroll, W. L. & Woerpel, K. A. Five-membered ring peroxide selectively initiates ferroptosis in cancer cells. *ACS. Chem. Biol.* **11**, 1305–1312 (2016).
11. Hanahan, D. & Weinberg, R. A. Hallmarks of cancer: the next generation. *Cell* **144**, 646–674 (2011).
12. Skouta, R. et al. Ferrostatins inhibit oxidative lipid damage and cell death in diverse disease models. *J. Am. Chem. Soc.* **136**, 4551–4556 (2014).
13. Zilka, O. et al. On the mechanism of cytoprotection by ferrostatin-1 and liproxstatin-1 and the role of lipid peroxidation in ferroptotic cell death. *ACS Cent. Sci.* **3**, 232–243 (2017).
14. Krainz, T. et al. A mitochondrial-targeted nitroxide is a potent inhibitor of ferroptosis. *ACS Cent. Sci.* **2**, 653–659 (2016).
15. Gaschler, M. M. & Stockwell, B. R. Lipid peroxidation in cell death. *Biochem. Biophys. Res. Commun.* **482**, 419–425 (2017).
16. Kagan, V. E. et al. Oxidized arachidonic and adrenic PEs navigate cells to ferroptosis. *Nat. Chem. Biol.* **13**, 81–90 (2017).
17. Shimada, K. et al. Global survey of cell death mechanisms reveals metabolic regulation of ferroptosis. *Nat. Chem. Biol.* **12**, 497–503 (2016).
18. Dixon, S. J. et al. Pharmacological inhibition of cystine-glutamate exchange induces endoplasmic reticulum stress and ferroptosis. *ELife* **3**, e02523 (2014).
19. Yin, J. et al. Cyanine-based fluorescent probe for highly selective detection of glutathione in cell cultures and live mouse tissues. *J. Am. Chem. Soc.* **136**, 5351–5358 (2014).
20. Ishii, T., Bannai, S. & Sugita, Y. Mechanism of growth stimulation of L1210 cells by 2-mercaptoethanol in vitro. Role of the mixed disulfide of 2-mercaptoethanol and cysteine. *J. Biol. Chem.* **256**, 12387–12392 (1981).
21. Toppo, S., Flohé, L., Ursini, F., Vanin, S. & Maiorino, M. Catalytic mechanisms and specificities of glutathione peroxidases: variations of a basic scheme. *Biochim. Biophys. Acta* **1790**, 1486–1500 (2009).
22. Beekman, A. C. et al. Stereochemistry-dependent cytotoxicity of some artemisinin derivatives. *J. Nat. Prod.* **60**, 325–330 (1997).
23. Beekman, A. C. et al. Artemisinin-derived sesquiterpene lactones as potential antitumour compounds: cytotoxic action against bone marrow and tumour cells. *Planta Med.* **64**, 615–619 (1998).
24. Burkhard, J. A., Wuitschik, G., Rogers-Evans, M., Müller, K. & Carreira, E. M. Oxetanes as versatile elements in drug discovery and synthesis. *Angew. Chem. Int. Ed. Engl.* **49**, 9052–9067 (2010).
25. Wuitschik, G. et al. Oxetanes in drug discovery: structural and synthetic insights. *J. Med. Chem.* **53**, 3227–3246 (2010).
26. Trost, B. M. & Bogdanow, M. J. New synthetic reactions—versatile cyclobutanone (spiroannelation) and gamma-butyrolactone (lactone annelation) synthesis. *J. Am. Chem. Soc.* **95**, 5321–5334 (1973).
27. Fujioka, H. et al. Reaction of the acetals with TESOTf-base combination; speculation of the intermediates and efficient mixed acetal formation. *J. Am. Chem. Soc.* **128**, 5930–5938 (2006).
28. Murai, A., Ono, M. & Masamune, T. Intramolecular cyclization of 3,4-epoxy alcohols—oxetane formation. *Bull. Chem. Soc. Jpn.* **50**, 1226–1231 (1977).
29. Biemann, K. & Seibl, J. Application of mass spectrometry to structure problems. 2. Stereochemistry of epimeric, cyclic alcohols. *J. Am. Chem. Soc.* **81**, 3149–3150 (1959).
30. Liu, Y. et al. Guanacastane-type diterpenoids with cytotoxic activity from *Coprinus plicatilis*. *Bioorg. Med. Chem. Lett.* **22**, 5059–5062 (2012).
31. Ki, D. W. et al. New antioxidant sesquiterpenes from a culture broth of *Coprinus echinosporus*. *J. Antibiot. (Tokyo)* **68**, 351–353 (2015).
32. Vilotijevic, I. & Jamison, T. F. Epoxide-opening cascades in the synthesis of polycyclic polyether natural products. *Angew. Chem. Int. Ed. Engl.* **48**, 5250–5281 (2009).
33. Hwang, C., Sinskey, A. J. & Lodish, H. F. Oxidized redox state of glutathione in the endoplasmic reticulum. *Science* **257**, 1496–1502 (1992).
34. Spangler, B. et al. A novel tumor-activated prodrug strategy targeting ferrous iron is effective in multiple preclinical cancer models. *J. Med. Chem.* **59**, 11161–11170 (2016).
35. Fontaine, S. D., DiPasquale, A. G. & Renslo, A. R. Efficient and stereocontrolled synthesis of 1,2,4-trioxolanes useful for ferrous iron-dependent drug delivery. *Org. Lett.* **16**, 5776–5779 (2014).
36. Davidson, B. S. Cytotoxic 5-membered cyclic peroxides from a plakortis sponge. *J. Org. Chem.* **56**, 6722–6724 (1991).
37. D'Ambrosio, M., Guerriero, A., Debitus, C., Waikedre, J. & Pietra, F. Relative contributions to antitumoral activity of lipophilic vs. polar reactive moieties in marine terpenoids. *Tetrahedr. Lett* **38**, 6285–6288 (1997).
38. Hurlocker, B., Miner, M. R. & Woerpel, K. A. Synthesis of silyl monoperoxyketals by regioselective cobalt-catalyzed peroxidation of silyl enol ethers: application to the synthesis of 1,2-dioxolanes. *Org. Lett.* **16**, 4280–4283 (2014).
39. Park, S. E. et al. Induction of apoptosis in MDA-MB-231 human breast carcinoma cells with an ethanol extract of *Cyperus rotundus* L. by activating caspases. *Oncol. Rep.* **32**, 2461–2470 (2014).
40. Yu, B. & Reynisson, J. Bond stability of the "undesirable" heteroatom-heteroatom molecular moieties for high-throughput screening libraries. *Eur. J. Med. Chem.* **46**, 5833–5837 (2011).
41. Nam, W. et al. Effects of artemisinin and its derivatives on growth inhibition and apoptosis of oral cancer cells. *Head Neck* **29**, 335–340 (2007).
42. Ooko, E. et al. Artemisinin derivatives induce iron-dependent cell death (ferroptosis) in tumor cells. *Phytomedicine.* **22**, 1045–1054 (2015).
43. Barnes-Seeman, D. et al. Metabolically stable *tert*-butyl replacement. *ACS Med. Chem. Lett.* **4**, 514–516 (2013).
44. Wang, X. et al. Spiro- and dispiro-1,2-dioxolanes: contribution of iron(II)-mediated one-electron vs two-electron reduction to the activity of antimalarial peroxides. *J. Med. Chem.* **50**, 5840–5847 (2007).
45. Yant, L. J. et al. The selenoprotein GPX4 is essential for mouse development and protects from radiation and oxidative damage insults. *Free. Radic. Biol. Med.* **34**, 496–502 (2003).
46. Hong, Y. et al. The role of selenium-dependent and selenium-independent glutathione peroxidases in the formation of prostaglandin $F_{2\alpha}$. *J. Biol. Chem.* **264**, 13793–13800 (1989).

47. Dansen, T. B., Wirtz, K. W. A., Wanders, R. J. A. & Pap, E. H. W. Peroxisomes in human fibroblasts have a basic pH. *Nat. Cell Biol.* **2**, 51–53 (2000).
48. Beasley, D. E., Koltz, A. M., Lambert, J. E., Fierer, N. & Dunn, R. R. The evolution of stomach acidity and its relevance to the human microbiome. *PLoS ONE* **10**, e0134116 (2015).
49. Creek, D. J., Chiu, F. C. K., Prankerd, R. J., Charman, S. A. & Charman, W. N. Kinetics of iron-mediated artemisinin degradation: effect of solvent composition and iron salt. *J. Pharm. Sci.* **94**, 1820–1829 (2005).
50. Wu, Y., Yue, Z. Y. & Wu, Y. L. Interaction of qinghaosu (artemisinin) with cysteine sulfhydryl mediated by traces of non-heme iron. *Angew. Chem. Int. Ed. Engl.* **38**, 2580–2582 (1999).

Acknowledgements

We thank C. Lin for assistance with NMR spectroscopy and mass spectrometry, C. Hu for X-ray analysis, along with the Materials Research Science and Engineering Center (MRSEC) program of the National Science Foundation (NSF) under Award Numbers DMR-0820341 and DMR-1420073, and J. Chung for assistance with cell culture. This research was supported by the Training Program in Molecular Biophysics Grant (T32GM008281 to M.M.G.), the National Cancer Institute (R35CA209896 and P01CA087497 to B.R.S), the National Institute of General Medical Sciences (1RO1GM118730 to K.A.W.), the National Heart, Lung, and Blood Institute (HL114453 to V.E.K. and Y.Y.T.), the National Institute of Allergy and Infectious Diseases (U19AI068021 to V.E.K. and Y.Y.T.) and the MRSEC Program of the National Science Foundation (DMR-1420073 to E.P.-P.). The Bruker Avance-400, 500 and 600 MHz spectrometers (NYU) were acquired through the support of the National Science Foundation (CHE-01162222).

Author contributions

M.M.G., A.A.A., H.L., B.R.S. and K.A.W. contributed to the writing of the manuscript. M.M.G., A.A.A., L.K.M., V.E.K., B.R.S. and K.A.W. designed and planned research. M.M.G., A.A.A., H.L., J.M.C., D.W.H., D.S.Z., P.H.B., Y.Y.T. and J.D.D. conducted in vitro biochemical and metabolomic assays. M.M.G, A.A.A., B.H., C.A.V., D.W.H. and A.J.L. collected and analyzed cell viability data. L.F.Y. performed quantitative PCR. A.A.A. and H.L. conducted NMR studies. A.A.A. conducted stability studies. H.L. and E.R. conducted western blotting experiments. A.A.A., B.H. and D.S.Z. synthesized $FINO_2$ and all structural analogues. A.Y.C. aided in furan synthesis. E.P.-P. aided in oxetane synthesis. M.A.F., A.V.B., V.V.S., A.J.L. and M.S.S. synthesized deuterated arachidonic acids. All authors have given their approval of the final version of the manuscript.

Competing interests

M.S.S. is the Chief Scientific Officer of Retrotrope, Inc.

Additional information

Supplementary information is available for this paper at https://doi.org/10.1038/s41589-018-0031-6.

Reprints and permissions information is available at www.nature.com/reprints.

Correspondence and requests for materials should be addressed to K.A.W. or B.R.S.

Publisher's note: Springer Nature remains neutral with regard to jurisdictional claims in published maps and institutional affiliations.

Methods

Cell lines and media. HT-1080 cells were obtained from ATCC and grown in DMEM with glutamine and sodium pyruvate (Corning 10-013) supplemented with 10% heat-inactivated FBS, 1% non-essential amino acids (Invitrogen) and 1% penicillin-streptomycin mix (Invitrogen). BJ-5ta (BJ-hTERT) cells were obtained from ATCC and grown in DMEM supplemented with 10% FBS and 1% penicillin-streptomycin. BJ-eLR cells were donated by the laboratory of W. Hahn at the Dana-Farber Cancer Institute and grown in the same medium as BJ-hTERT cells. CAKI-1 cells were purchased from ATCC and grown in RPMI medium supplemented with 10% FBS and 1% penicillin-streptomycin. All cells were maintained in a humidified environment at 37 °C and 5% CO_2 in a tissue incubator.

Chemical synthesis of $FINO_2$ analogs. Synthetic protocols are described in the Supplementary Note.

$FINO_2$ analog potency measurement. BJ-eLR, BJ-hTERT or CAKI-1 cells were plated at 10,000 cells per well in white 96-well plates in technical triplicates and incubated for 24 h to allow cell adhesion. The cells were then treated with either vehicle (DMSO), $FINO_2$ or a $FINO_2$ analog at 5, 10, 25, 50 or 100 μM concentrations. The cells were returned to the cell culture incubator for 48 h. CellTiter-Glo (Promega) was used according to the manufacturer's protocol. Luminescence was read on a Bioteck Microplate Reader. All cell viability data were normalized to the DMSO vehicle condition. Experiments were performed three independent times with different passages for each cell line. EC_{50} values and error values were computed using Prism 7.0 (GraphPad).

Ferroptosis rescue and sensitivity modulation. Three thousand cells were seeded per well in black, clear-bottom 384-well plates (Corning) and allowed to adhere overnight. For ferroptosis rescue assays, the medium was replaced on the following day with 50 μL of growth medium and 5 μL medium containing a ferroptosis inducer and a dilution series of a protective molecule. The final concentration of ferroptosis inducers was 10 μM erastin, 10 μM $FINO_2$, 2 μM RSL3 and 5 μM FIN56 unless otherwise noted. For sensitivity modulation experiments, cells were cotreated with a fixed concentration of the modulating compound and a dilution series of the ferroptosis inducer. For deuterated arachidonic acids, cells were incubated in medium containing 80 μM of a deuterated arachidonic acid overnight to allow incorporation into cellular membranes. The following day cells were treated with a dilution series of ferroptosis inducer. In all cases, after 24 h incubation with ferroptosis inducer, 6.1 μL of Presto Blue (ThermoFisher) were added. Cells were incubated for an additional 3 h and the Presto Blue fluorescence intensity was measured using a Victor X5 plate reader (PerkinElmer) (ex/em 530/590). Background (no cells) fluorescence was subtracted and the resulting fluorescence intensities were averaged between biological replicates. From these data, dose–response curves and EC_{50} values were computed using Prism 7.0 (GraphPad).

C11-BODIPY lipid peroxidation measurement. The day before the experiment, 600,000 HT-1080 cells were seeded in six-well plates and allowed to adhere overnight at 37 °C. On the day of the experiment, cells were treated with DMSO, erastin (10 μM) or $FINO_2$ (10 μM) with or without DFO (100 μM) and incubated for 6 h at 37 °C. Cells were trypsinized, washed, suspended in HBSS containing 1.5 μM C11-BODIPY (ThermoFisher) and incubated at 37 °C for 15 min. Cells were pelleted and resuspended in HBSS. Fluorescence intensity was measured on the FL1 channel with gating to record live cells only (gate constructed from DMSO treatment group). A minimum of 10,000 cells was analyzed per condition.

Reduced glutathione measurement. Ten million HT-1080 cells were treated with 5 μM erastin, 10 μM $FINO_2$, 500 nM RSL3 or vehicle. Cells were harvested after 1.5 h (RSL3) or 6 h (vehicle, erastin, $FINO_2$) and lysed using ice-cold PBS containing 0.5% Nonidet P-40. Samples were centrifuged for 15 min at 4 °C at 17,000*g*. The resulting supernatant was deproteinized using a deproteinizing kit (ab2047080, Abcam) and kept on ice. Reduced GSH levels were determined using GSH/GSSG Ratio Detection Assay Kit (Fluorometric - Green) (ab138881, Abcam) following the manufacturer's protocol.

TBARS measurement. Twenty million HT-1080 cells were treated with 5 μM erastin or 10 μM $FINO_2$ with or without 2 μM ferrostatin-1 and harvested after 6 h into 1 mL PBS. Samples were sonicated and the homogenate was stored on ice. TBARS were measured using a TBARS (TCA Method) Assay Kit (Cayman 700870) following the manufacturer's protocol.

qPCR. HT-1080 cells were treated with either 10 μM erastin, 10 μM $FINO_2$ or 2 μM RSL3 for 5 h. RNA was extracted using the Qiashredder and Qiagen RNeasy Mini kits (Qiagen) according to the manufacturer's protocol. For each sample 2 μg of RNA were used as input for each reverse transcription reaction, performed using the TaqMan RT kit (Applied Biosystems/Life Technologies Corp., Foster City, CA). Quantitative PCR reactions were performed using Power SYBR Green PCR Master Mix (Applied Biosystems). Triplicate samples per condition were analyzed on a ViiA 7 qPCR instrument (Thermo Fischer) using absolute quantification settings. Differences in mRNA levels compared to *ACTB* internal reference control were computed between control and experimental conditions using the ΔΔCt method.

HSQC NMR. Uniformly ^{15}N-labeled $GPX4^{U46C}$ was expressed in and purified from *Escherichia coli*. For HSQC of GPX4 with FINO2, 50 μM ^{15}N-labeled GPX4 was preincubated with 500 μM $FINO_2$ for 6 h at room temperature in buffer (100 mM MES, 5 mM TCEP, pH 6.5). For HSQC of GPX4 with RSL3, since solubility of RSL3 in aqueous solution is low, 10 μM ^{15}N-labeled GPX4 was preincubated with 100 μM RSL3 for 12 h at 4 °C. Then the protein solution was concentrated to 50 μM before testing. D_2O (10%) was added for the field frequency lock. The ^1H-^{15}N HSQC spectra were collected on Bruker Avance III 500 Ascend (500 MHz) spectrometers at ambient temperature. The ^1H carrier frequency was positioned at the water resonance. The ^{15}N carrier frequency was positioned at 115 ppm. The spectral width in the ^1H dimension was 7,500 Hz and the width in the ^{15}N dimension was 1,824.6 Hz. Suppression of water signal was accomplished using the WATERGATE sequence. Heteronuclear decoupling was accomplished using GARP decoupling scheme.

Western blotting. HT-1080 cells were seeded at 800,000 per well in a 60-mm plate and allowed to adhere overnight. Cells were then treated with 100 μM α-tocopherol and either 1 μM RSL3, 10 μM erastin, 5 μM FIN56, 10 μM $FINO_2$ or vehicle for 10 h. Cells were harvested with trypsin (Invitrogen, 25200-114), pelleted, and frozen at −80 °C. Cell pellets were thawed, lysed, blotted and imaged as previously described[3]. In particular, for this experiment, the set of 15 pellets was run on a single gel. Ultimately, two gels were run and quantified from a total of six biological replicates (30 pellets in total). For the other proteins of interest, experiments were performed in biological triplicate. Antibodies used were GPX4 (Abcam, ab125066, 1:250 dilution), ferritin light chain (Santa Cruz, sc-390558, 1:1,000 dilution), IRP2 (Nous Biological, NB100-1798, 1:1,000 dilution), transferrin receptor 1 (CD71, TFRC, Cell Signaling, 13113, 1:1,000 dilution), actin (Cell Signaling, D18C11, 1:3,000 dilution), α-tubulin (Santa Cruz, sc-32293, 1:3,000 dilution) and GAPDH (Santa Cruz, sc-47724, 1:10,000 dilution). Results were quantified using a LI-COR Odyssey CLx IR scanner and GraphPad Prism 7.

Decomposition of $FINO_2$ by $FeSO_4$. An NMR tube was charged with $FINO_2$ (5.0 mg, 0.020 mmol) and D_2O:CD_3CN (1:1, 0.04 M per solvent). The NMR was preheated to 37 °C and the ^1H spectrum was acquired. Then $FeSO_4{\cdot}7H_2O$ (11 mg, 0.039 mmol) was added. After 12 h, a ^1H spectrum was acquired at room temperature.

Colorimetric iron oxidation. In a clear 96-well plate, 4 μL of a 25 mM DMSO solution of test compound was added to 196 μL of a 2:1 (v/v) solution of water and DMSO containing 500 μM $FeCl_2$. This mixture was incubated at 37 °C for 1 h. Five microliters of a 20 mM stock of FerroZine (Sigma Aldrich) was added. Absorbance was measured at 567 nm.

LC–MS GPX4 activity assay. For experiments performed on whole cells, 20 million HT-1080 cells were treated with vehicle (DMSO), erastin (10 μM), $FINO_2$ (10 μM) or FIN56 (5 μM) for 6 h, or RSL3 (0.5 μM) for 2 h. Cells were harvested by trypsinization, washed twice in PBS and resuspended in lysis buffer (25 mM sodium phosphate, 125 mM NaCl, 1 mM EDTA, 0.1 mM deferoxamine, 25 μM butylated hydroxytoluene, 0.3% Triton-X 100 and protease inhibitor (1 tablet per 10 mL)). Cells were lysed by sonication and cleared of insoluble components by centrifugation at 14,000*g* for 10 min at 4 °C. For cell-free assays, HT-1080 cells were harvested by trypsinization, washed twice in PBS and resuspended in ice-cold NP40 lysis buffer (10 mM Tris/Cl pH 7.5, 150 mM NaCl, 0.5 mM EDTA, 0.5% NP-40, 5 mM TCEP and protease inhibitor (1 tablet per 10 mL)). Cells were lysed by placing on ice for 30 min with extensive pipetting every 10 min and then centrifuging at 14,000*g* for 10 min at 4 °C. The protein concentration of each sample was determined using the Bradford assay. For cell-free experiments, cell lysate containing 200 μg protein was separately preincubated with vehicle (DMSO, 0.2%), erastin (10 μM), RSL3 (20/200 μM) or $FINO_2$ (40/400 μM) for 10 min at 37 °C in 500 μL GXP4 reaction buffer (25 mM sodium phosphate, 125 mM NaCl, 1 mM EDTA, 0.1 mM deferoxamine, 0.1% Triton X-100 and 5 mM TCEP). Otherwise, PCOOH reduction reactions contained 200 μg of protein from treated groups, 5 mM reduced glutathione, 10 μM PCOOH and sufficient reaction buffer to raise the volume to 500 μL (reaction buffer: 25 mM sodium phosphate, 125 mM NaCl, 1 mM EDTA, 0.1 mM deferoxamine, 0.1% Triton X-100). Reactions were incubated at 37 °C for 30 min and then extracted with 1 mL of chloroform:methanol mixture (2:1 v/v). The organic portion was isolated and evaporated. Dry extracted materials were reconstituted in methanol. The samples were analyzed by LC–MS for PCOOH content as described previously[4,17].

MS analysis of phospholipids. Lipids were extracted by using Folch's procedure[51]. Lipid phosphorus was determined by a micro-method[52]. MS analysis of phospholipids was performed on a Q-Exactive hybrid-quadrupole-orbitrap mass spectrometer (ThermoFisher Scientific) as previously described[53]. Phospholipids were separated on a normal phase column (Silica Luna 3 μm, 100 A, 150 × 2 mm, (Phenomenex, Torrance CA)) at 35 °C using gradient solvents containing 5 mM

ammonium acetate (A: *n*-hexane:2-propanol:water 43:57:1 (v/v/v); B: *n*-hexane:2-propanol:water, 43:57:8 (v/v/v)). The gradient conditions (all linear) were as follows: 0–23 min (10% B to 32% B); 23–32 min (32% B to 65% B); 32–35 min (65% B to 100% B); 35–62 min (hold at 100% B); 62–64 min (100% B to 10% B); 64–80 min (10% B). Flow rate was maintained at 200 µL/min except for the 35–62 min time frame, where the flow rate was increased to 225 µl/min. MS analysis was performed in negative ion mode at a resolution of 140,000 for the full MS scan in data-dependent mode. The scan range for MS analysis was 400–1,800 *m*/*z* with a maximum injection time of 128 ms using one microscan. An isolation window of 1.0 Da was set for the MS and MS2 scans. Capillary spray voltage was set at 3.5 kV and capillary temperature was 320 °C. The S-lens Rf level was set to 60. Analysis of LC–MS data was performed using the software package Compound Discoverer (ThermoFisher Scientific, San Jose, CA) with an in-house-generated analysis workflow and oxidized phospholipid database.

NADPH quantification. NADPH levels were analyzed using an Amplite fluorimetric NADP/NADPH ratio assay kit (AAT Bioquest). One million HT-1080 cells were seeded in 100-mm tissue culture dishes for 16 h. Cells were treated with either vehicle or a ferroptosis inducer (0.1% DMSO for 8 h, 5 µM FIN56 for 8 h, 10 µM erastin for 8 h, 0.5 µM RSL3 for 3 h, 10 µM FINO2 for 8 h). After treatment, the cells were trypsinized, pelleted, lysed and analyzed for NADPH levels in the same way as described before[54]. The concentrations of these metabolites were normalized to the amount of total protein. Measurements were done in biological triplicates. NADPH levels of all samples were normalized to DMSO vehicle control.

In vitro microsomal stability assay. To a 96-well round bottom polypropylene plate (PerkinElmer 6008190) was added phosphate buffer (182.2 µL, pH 7.4, 100 mM) followed by NADPH-regenerating system solution A (10 µL) and NADPH regenerating system solution B (2 µL) (Corning Gentest 3 P NADPH regenerating system solution A (451220) and B (451200)). A stock solution of $FINO_2$ (0.8 µL, 5 mM) or ferrostatin-1 (Fer-1) (positive control, 0.8 µL, 5 mM) in methanol was added and the mixture was warmed to 37 °C for 5 min. Mouse microsomes (CD-1, 20 mg/mL, Life Technologies) or human microsomes (pooled 50 donors, 20 mg/mL, ThermoFisher Scientific) (5 µL, thawed in 37 °C bead bath before use) were added. At selected time points (0, 1, 5, 10, 20, 30, 60 and 120 min) aliquots (15 µL) were withdrawn from the plate and quenched upon addition to cold methanol (60 µL) containing a terfenadine internal standard (1.25 mM) in a 96-well polypropylene plate kept on ice. The samples were centrifuged at 1,600*g* for 5 min at 4 °C. The supernatant (40 µL) was withdrawn and transferred to a sample vial with insert.

In vitro plasma stability assay. Mouse and human plasma from GeneTex (mouse: GTX73236, human: GTX73265) aliquoted and stored at –80 °C was thawed in a 37 °C bead bath and centrifuged at 900*g* for 10 min at 10 °C to remove any particulates. The particulate-free plasma was diluted in phosphate buffer (pH 7.4, 100 mM) to a final plasma concentration of 50%. The 50% plasma solution (195 µL) was added to a 96-well round-bottom polypropylene plate (PerkinElmer 6008190) and the mixture was warmed to 37 °C for 5 min. A stock solution of $FINO_2$ (5 µL, 800 µM), ferrostatin-1 (Fer-1) (negative control 5 µL, 800 µM) or lovastatin (positive control, 5 µL, 800 µM) DMSO was added. At selected time points (0, 5, 15, 30, 60, 120, 180 and 360 min) aliquots (15 µL) were withdrawn from the plate and quenched upon addition to cold acetonitrile (60 µL) containing a terfenadine internal standard (1.25 mM) in a 96-well polypropylene plate kept on ice. The samples were centrifuged at 1,600*g* for 5 min at 4 °C. The supernatant (40 µL) was withdrawn and transferred to a sample vial with insert.

LC–MS analysis of in vitro pharmacokinetic studies. LC–MS analysis was performed on a platform comprising a Thermo Scientific Dionex Ultimate 3000 and a Bruker amaZon SL equipped with an electrospray ionization source controlled by Bruker Hystar 3.2. Chromatographic separation was performed by injecting 5 mL of the sample onto an Agilent Eclipse Plus C18 column (2.1 mm × 50 mm, 3µm particle size) maintained at 20 °C. The flow rate was maintained at 400 mL/min. The initial flow conditions were 80% solvent A (95:5:0.1 water:methanol:acetic acid with 10 mM ammonium acetate) and 20% solvent B (methanol containing 0.1% acetic acid). Solvent B was maintained at 20% for the first minute of the run and was raised to 80% over 0.50 min. Solvent B was raised to 100% by 5 min and was lowered back to initial conditions (20%) by 8.750 min with a total run time of 12.0 min. The retention times and *m*/*z* values are summarized in Supplementary Table 1.

The area of the base peak chromatogram for each compound was measured at each time-point and compared against the zero-minute time point to calculate the percentage of compound remaining at each time point. For samples where the percentage of compound remaining was greater than 100% at the second time point, the second time point was used to calculate the percentage of compound remaining. The data were plotted in Prism 7 and the data fit with a one-phase linear decay model with y_0 value set to 100 to calculate the half-life. For compounds with half-lives greater than 2 h, the percentage of compound remaining after 120 min is reported.

Statistical analysis. The data reported in this study represent the mean and s.d. of at least three independent experiments measured in triplicate, unless otherwise stated in the figure legend. For statistical analyses, ANOVA and two-tailed Student's *t*-tests were conducted to assess whether a significant difference exists between two groups of samples. A *P* value of less than 0.05 was considered statistically significant. All statistical tests were carried out using Prism 7 software (GraphPad).

Data availability. The data that support the findings of this study are available from the corresponding authors upon request.

References

51. Folch, J., Lees, M. & Sloane Stanley, G. H. A simple method for the isolation and purification of total lipides from animal tissues. *J. Biol. Chem.* **226**, 497–509 (1957).
52. Boettcher, C., Pries, C. & Vangent, C. M. A rapid and sensitive sub-micro phosphorus determination. *Anal. Chim. Acta* **24**, 203–204 (1961).
53. Tyurina, Y. Y. et al. A mitochondrial pathway for biosynthesis of lipid mediators. *Nat. Chem.* **6**, 542–552 (2014).
54. Shimada, K., Hayano, M., Pagano, N. C. & Stockwell, B. R. Cell-line selectivity improves the predictive power of pharmacogenomic analyses and helps identify NADPH as biomarker for ferroptosis sensitivity. *Cell Chem. Biol.* **23**, 225–235 (2016).

nature research

Corresponding author(s): Brent Stockwell, Keith Woerpel

☐ Initial submission ☐ Revised version ☒ Final submission

Life Sciences Reporting Summary

Nature Research wishes to improve the reproducibility of the work that we publish. This form is intended for publication with all accepted life science papers and provides structure for consistency and transparency in reporting. Every life science submission will use this form; some list items might not apply to an individual manuscript, but all fields must be completed for clarity.

For further information on the points included in this form, see Reporting Life Sciences Research. For further information on Nature Research policies, including our data availability policy, see Authors & Referees and the Editorial Policy Checklist.

Experimental design

1. Sample size

Describe how sample size was determined.

No sample size calculations were performed. Experiments were performed with three replicates for each treatment group in order to observe variance. Experiments were performed three times to ensure reproducibility and accuracy.

2. Data exclusions

Describe any data exclusions.

No exclusions

3. Replication

Describe whether the experimental findings were reliably reproduced.

All attempts at replication were successful

4. Randomization

Describe how samples/organisms/participants were allocated into experimental groups.

Prior to beginning an experiment, cells were seeded/allocated into wells in the same manner for each sample group. When an experiment was commenced, groups of cells were allocated into treatment groups without pattern or bias. This ensured that each treatment group in an experiment were identical (within the inherent variation caused by cell seeding).

5. Blinding

Describe whether the investigators were blinded to group allocation during data collection and/or analysis.

No Blinding was used

Note: all studies involving animals and/or human research participants must disclose whether blinding and randomization were used.

6. Statistical parameters

For all figures and tables that use statistical methods, confirm that the following items are present in relevant figure legends (or in the Methods section if additional space is needed).

n/a	Confirmed
☐	☒ The exact sample size (*n*) for each experimental group/condition, given as a discrete number and unit of measurement (animals, litters, cultures, etc.)
☐	☒ A description of how samples were collected, noting whether measurements were taken from distinct samples or whether the same sample was measured repeatedly
☐	☒ A statement indicating how many times each experiment was replicated
☐	☒ The statistical test(s) used and whether they are one- or two-sided (note: only common tests should be described solely by name; more complex techniques should be described in the Methods section)
☐	☒ A description of any assumptions or corrections, such as an adjustment for multiple comparisons
☐	☒ The test results (e.g. *P* values) given as exact values whenever possible and with confidence intervals noted
☐	☒ A clear description of statistics including central tendency (e.g. median, mean) and variation (e.g. standard deviation, interquartile range)
☐	☒ Clearly defined error bars

See the web collection on statistics for biologists for further resources and guidance.

Software

Policy information about availability of computer code

7. Software

Describe the software used to analyze the data in this study.	Prism 7 was used for line-fitting, FlowJo 10.1 was used for flow cytometry analysis, Topspin and MestreNova were used for NMR analysis, Compound Discoverer was used for MS phospholipid analysis.

For manuscripts utilizing custom algorithms or software that are central to the paper but not yet described in the published literature, software must be made available to editors and reviewers upon request. We strongly encourage code deposition in a community repository (e.g. GitHub). *Nature Methods* guidance for providing algorithms and software for publication provides further information on this topic.

Materials and reagents

Policy information about availability of materials

8. Materials availability

Indicate whether there are restrictions on availability of unique materials or if these materials are only available for distribution by a for-profit company.	Unique materials used in this study (RSL3, FINO2, FINO2 analogues, deuterated arachidonic acids) were synthesized by the authors and are available upon reasonable request. All other reagents were obtained commercially.

9. Antibodies

Describe the antibodies used and how they were validated for use in the system under study (i.e. assay and species).	The antibody for Gpx4 was obtained commercially from abcam (abcam, #ab125066); anti-GAPDH was obtained commercially from Santa Cruz biotech # sc-47724; anti-Ferritin Light Chain was obtained commercially from Santa Cruz biotech #sc-390558; anti-IRP2 was obtained commercially from Nous Biology #NB1001798; anti-Transferrin receptor 1 was obtained commercially from Cell Signaling #13113; anti-Actin was obtained commercially from Cell Signaling #D18C11; anti-alpha-tublin was obtained commercially from Santa Cruz biotech #sc-32293. All antibodies were used without further validation.

10. Eukaryotic cell lines

a. State the source of each eukaryotic cell line used.	HT-1080, BJ-hTERT, and CAKI-1 were obtained from ATCC; BJ-eLR cells were donated from the lab of William Han at the Dana Farber Cancer Institute.
b. Describe the method of cell line authentication used.	None of the cell lines have yet been identified
c. Report whether the cell lines were tested for mycoplasma contamination.	Cells were tested for mycoplasma pior to used with a PCR-based kit (Sigma). Cells were considered mycoplasma-free as no mycoplasma DNA amplified
d. If any of the cell lines used are listed in the database of commonly misidentified cell lines maintained by ICLAC, provide a scientific rationale for their use.	No lines from this database were used in this study

Animals and human research participants

Policy information about studies involving animals; when reporting animal research, follow the ARRIVE guidelines

11. Description of research animals

Provide details on animals and/or animal-derived materials used in the study.	None used in this study

Policy information about studies involving human research participants

12. Description of human research participants

Describe the covariate-relevant population characteristics of the human research participants.	None used in this study